Variable flavor number parton distributions and weak gauge and Higgs boson production at hadron colliders at next-to-next-to-leading order of QCD

P. Jimenez-Delgado and E. Reya

Universität Dortmund, Institut für Physik D-44221 Dortmund, Germany

(Received 9 September 2009; published 11 December 2009)

Based on our recent next-to-next-to-leading order (NNLO) dynamical parton distributions as obtained in the ''fixed flavor number scheme,'' we generate radiatively parton distributions in the ''variable flavor number scheme'' where the heavy-quark flavors (c, b, t) also become massless partons within the nucleon. Only within this latter factorization scheme are NNLO calculations feasible at present, since the required partonic subprocesses are only available in the approximation of massless initial-state partons. The NNLO predictions for gauge boson production are typically *larger* (by more than 1σ) than the next-to-leading order (NLO) ones, and rates at LHC energies can be predicted with an accuracy of about 5%, whereas at Tevatron they are more than 2σ above the NLO ones. The NNLO predictions for standard model Higgs-boson production via the dominant gluon fusion process have a total (parton distribution function and scale) uncertainty of about 10% at LHC which almost doubles at the lower Tevatron energies; they are typically about 20% larger than the ones at NLO but the total uncertainty bands overlap.

DOI: 10.1103/PhysRevD.80.114011 PACS numbers: 12.38.−t, 12.38.Bx, 13.85.−t

I. INTRODUCTION

Parton distributions and their implications have been recently studied within the dynamical (radiative) parton model approach up to next-to-next-to-leading order (NNLO) of QCD [1]. Here the predicted steep small Bjorken-x behavior of structure functions is mainly due to QCD dynamics at $x \lesssim 10^{-2}$, since the parton distributions at $Q^2 \gtrsim 1$ GeV^2 are QCD radiatively generated from *valencelike* positive definite input distributions at an optimally determined low input scale $Q_0^2 \equiv \mu^2 < 1$ GeV^2. (''Valencelike'' refers to $a_f > 0$ for *all* input distributions $xf(x, \mu^2) \propto x^{a_f}(1-x)^{b_f}$, i.e., not only the valence but also the sea and gluon input densities vanish at small x.)[1] Such analyses are usually performed within the framework of the so-called ''fixed flavor number scheme'' (FFNS) where, besides the gluon, only the light quark flavors $q = u, d, s$ are considered as genuine, i.e., massless partons within the nucleon. This factorization scheme is fully predictive in the heavy-quark $h = c, b, t$ sector where the heavy-quark flavors are produced entirely perturbatively as final state quantum fluctuations in the strong field generated by the initial light quarks and gluons. Here the full heavy-quark mass $m_{c,b,t}$ dependence is taken into account in the production cross sections, as required experimentally [2–5], in particular, in the threshold (th) region. However, even for very large values of Q^2, $Q^2 \gg m_{c,b}^2$, these FFNS predictions up to next-to-leading order (NLO) are in remarkable agreement [6,7] with deep inelastic scattering (DIS) data and, moreover, are perturbatively stable despite the common belief that ''noncollinear'' logarithms $\ln(Q^2/m_h^2)$ have to be resummed for $h = c, b$, and eventually t. This agreement with the experiment even at $Q^2 \gg m_h^2$ indicates that there is *little* need to resum these supposedly ''large logarithms,'' which is of course in contrast to the genuine collinear logarithms appearing in light (massless) quark and gluon hard scattering processes. It should be mentioned that, so far, the heavy NNLO $\mathcal{O}(\alpha_s^3)$ 3-loop corrections to $F_{2,L}$ have been calculated only asymptotically for $Q^2 \gg m_h^2$ [8–11].

In many situations, calculations within this factorization scheme become unduly complicated (for a recent discussion, see [12]). Thus it is advantageous to consider the so-called ''variable flavor number scheme'' (VFNS) despite the somewhat questionable resummations of heavy-quark mass effects using massless evolution equations, starting at unphysical ''thresholds'' $Q^2 = m_h^2$. Here the heavy quarks (c, b, t) are considered to be massless partons within the nucleon as well, with their distributions $h(x, Q^2) = \bar{h}(x, Q^2)$ being generated, up to NLO, from the boundary conditions $h(x, m_h^2) = \bar{h}(x, m_h^2) = 0$, and at NNLO from $h(x, m_h^2) = \bar{h}(x, m_h^2) = \mathcal{O}(\alpha_s^2)$ as will be explicitly given in the next section. Thus this factorization scheme is characterized by increasing the number of flavors n_f of massless partons by one unit at $Q^2 = m_h^2$ starting from $n_f = 3$ at $Q^2 = m_c^2$. Hence the $n_f > 3$ ''heavy'' quark distributions are perturbatively uniquely generated from the $n_f - 1$ ones via the massless renormalization group Q^2 evolutions (see,

[1]Alternatively, in the common ''standard'' approach the input scale is fixed at some arbitrarily chosen $Q_0^2 > 1$ GeV^2 and the corresponding input distributions are less restricted. For example, the observed *steep* small-x behavior ($a_f < 0$) of structure functions and consequently of the gluon and sea distributions has to be *fitted*. Furthermore the associated uncertainties encountered in the determination of the parton distributions turn out to be larger, particularly in the small-x region, than in the more restricted dynamical radiative approach where, moreover, the evolution distance (starting at $Q_0^2 < 1$ GeV^2) is sizably larger (see, e.g., [1] and references therein.)

e.g. [13,14]; a comparative qualitative and quantitative discussion of this zero-mass VFNS and the FFNS has been recently presented in [12]). Eventually one nevertheless has to *assume* that these massless heavy quark distributions are relevant asymptotically and that they correctly describe the asymptotic behavior of DIS structure functions for scales $Q^2 \gg m_h^2$. However, for most experimentally accessible values of Q^2, in particular, around the threshold region of heavy-quark ($h\bar{h}$) production, effects due to *finite* heavy-quark masses m_h can *not* be neglected. One therefore needs an improvement of this zero-mass VFNS where heavy-quark, mass-dependent corrections are maintained in the hard cross sections. Such improvements are generally referred to as the general-mass VFNS and there exist various different model-dependent ways of implementing the required m_h dependence [15–28].[2] These factorization schemes interpolate between the zero-mass VFNS (assumed to be correct asymptotically) and the (experimentally required) FFNS used for our previous analysis [1].

In order to avoid any such model ambiguities we shall generate in the next section the heavy zero-mass VFNS distributions using our unique NNLO dynamical FFNS distributions [1] as input at $Q^2 = m_c^2$. This will considerably ease the otherwise unduly complicated calculations in the FFNS of gauge- and Higgs-boson production and heavy-quark production at collider energies, or the calculation of weak charged-current (anti)neutrino-nucleon cross sections at ultrahigh neutrino energies, for example. It has been recently shown [12] that for situations where the invariant mass of the produced system (cW, tW, $t\bar{b}$, Higgs-bosons, etc.) exceeds by far the mass of the participating heavy flavor, the VFNS predictions deviate rather little from the FFNS ones, typically by about 10% which is within the margins of renormalization and factorization scale uncertainties, and ambiguities related to presently available parton distributions. Let us consider, for example, hadronic $W^{\pm}$ production. The relevant heavy-quark contributions at leading order (LO) have to be calculated via $g\bar{s}(\bar{d}) \to \bar{c}W^+$, $gu \to bW^+$ in the (fully massive) FFNS as compared to the much simpler quark fusion subprocesses $c\bar{s}(\bar{d}) \to W^+$, $\bar{b}u \to W^+$ in the VFNS, etc. Here nonrelativistic contributions from the threshold region in the FFNS are suppressed due to $\sqrt{\hat{s}_{\rm th}}/m_{c,b} \simeq M_W/m_{c,b} \gg 1$. Similarly, hadronic single top production via W-gluon fusion [29] requires in the FFNS the calculation of the subprocess $ug \to dt\bar{b}$ at LO and of $ug \to dt\bar{b}g$, etc., at NLO; in the VFNS one needs merely $ub \to dt$ at LO and $ub \to dtg$, etc., at NLO, using massless initial-state partons. Again, $\sqrt{\hat{s}_{\rm th}}/m_b \simeq m_t/m_b \gg 1$ and thus the FFNS and VFNS results are not too different. A similar agreement is obtained for hadronic (heavy) Higgs-boson production where the LO FFNS subprocess $gg \to b\bar{b}H$ has to be compared with the $b\bar{b}$ fusion subprocess (for massless initial-state partons) in the VFNS starting with $b\bar{b} \to H$ at LO. [$H = H^0_{\rm SM}$; h^0, H^0, A^0 denote the standard model (SM) Higgs-boson or a light scalar h^0, a heavy scalar H^0, and a pseudoscalar A^0 of supersymmetric theories with $M_H \gtrsim 100$ GeV.] Again, $\sqrt{\hat{s}_{\rm th}}/m_b = (2m_b + M_H)/m_b \gg 1$ in the FFNS which indicates that the simpler LO, NLO, and NNLO-VFNS $b\bar{b}$ fusion processes do provide reliable predictions. (Notice that these situations are very different from DIS heavy-quark $h\bar{h}$ production via $\gamma^* g \to h\bar{h}$, etc., where $\sqrt{\hat{s}_{\rm th}}/m_h = 2$ is not sufficiently large to exclude significant contributions from the threshold region and therefore the VFNS predictions deviate sizably from the FFNS ones [12].)

Within the present intrinsic theoretical uncertainties we can therefore rely on our uniquely generated NNLO-VFNS parton distribution functions (pdfs) where, moreover, the required NNLO cross sections for massless initial-state partons are, in contrast to the fully massive FFNS, available in the literature for a variety of important production processes. The perturbative stability of the NNLO predictions, when compared with the ones based on our dynamical NLO-VFNS pdfs [12], will be furthermore studied in the next section for the hadronic production of $W^{\pm}$ and Z^0 bosons, as well as of the SM Higgs boson at the Tevatron and at LHC. Our conclusions are summarized in Sec. III. Finally, the Mellin n moments of the renormalized heavy-quark flavor operator matrix elements relevant for the generation of the VFNS pdfs at NNLO are summarized in the Appendix.

II. HEAVY FLAVOR PARTON DISTRIBUTIONS AND THEIR IMPLICATIONS AT HIGH ENERGY COLLIDERS

Commonly, the flavor transitions $n_f \to n_f + 1$ are made when the factorization scale equals the (pole) mass of the heavy quarks, $Q^2 = m_h^2$, and the pdfs for $n_f + 1$ flavors are defined from the light flavor pdfs and the massive operator matrix elements for n_f light flavors. In Mellin n-moment space, the heavy-quark pdfs can then be expressed in terms of the original light ones at NNLO as

$$(h + \bar{h})_{n_f+1}(n, m_h^2) = a_s^2[\tilde{A}^{\rm PS,(2)}_{hq}(n)\Sigma_{n_f}(n, m_h^2) + \tilde{A}^{\rm S,(2)}_{hg}(n) g_{n_f}(n, m_h^2)], \quad (1)$$

$(h - \bar{h})_{n_f+1}(n, m_h^2) = 0$, and the remaining matching conditions for the light pdfs and the gluon distribution read

[2]Notice that it is rather superfluous to argue about the best choice of a factorization scheme since the scheme choice remains merely a theoretical convention as long as there are no observable signatures which allow one to uniquely distinguish between the FFNS and any version of a general-mass VFNS (except the strictly massless VFNS which has been known to be experimentally inadequate for a very long time).

$$(q \pm \bar{q})_{n_f+1}(n, m_h^2) = (q \pm \bar{q})_{n_f}(n, m_h^2) + a_s^2 A_{qq,h}^{\mathrm{NS},(2)}(n)(q \pm \bar{q})_{n_f}(n, m_h^2), \quad (2)$$

$$g_{n_f+1}(n, m_h^2) = g_{n_f}(n, m_h^2) + a_s^2[A_{gq,h}^{\mathrm{S},(2)}(n)\Sigma_{n_f}(n, m_h^2) + A_{gg,h}^{\mathrm{S},(2)}(n) g_{n_f}(n, m_h^2)], \quad (3)$$

with the moments of the flavor singlet quark distribution being given by

$$\Sigma_{n_f}(n, Q^2) = \int_0^1 dx x^{n-1} \sum_{k=1}^{n_f} [q_k(x, Q^2) + \bar{q}_k(x, Q^2)], \quad (4)$$

where $q_1 \equiv u$, $q_2 \equiv d$, etc. The coefficients $A^{(2)}(x)$ of the operator matrix elements have been originally calculated in [16] and their Mellin moments $A^{(2)}(n)$ have been analyzed and given in [8,11,30]. Because of our choice $Q^2 = m_h^2$ for the thresholds, only the scale-independent parts of the expressions for $A^{(2)}(n)$ are needed which, for completeness, will be summarized in the Appendix. The strong coupling $a_s \equiv \alpha_s(Q^2)/4\pi$ is matched at the various thresholds $Q^2 = m_h^2$ in the standard way as recapitulated in [1] with $\alpha_s(M_Z^2) = 0.1124$ as obtained in our dynamical scenario [1] using $m_c = 1.3$ GeV, $m_b = 4.2$ GeV, and $m_t = 175$ GeV. Our choice for the input of the heavy VFNS distributions in (1) are the unique NNLO dynamical FFNS distributions [1] at $Q^2 = m_c^2$, as obtained from the NNLO evolution of our valencelike input distributions at $Q^2 = \mu^2 = 0.55$ GeV^2 (see Table I of [1]). The resulting VFNS predictions at scales $Q^2 \gg m_h^2$ should become insensitive to this input selection [14], since asymptotically the VFNS pdfs are dominated by their radiative evolution rather than by the specific input at $Q^2 = m_h^2$, i.e., because of the long evolution distance input differences get evolved away at $Q^2 \gg m_h^2$ where the universal perturbative QCD splittings dominate.

For illustration we show in Fig. 1 our NNLO charm and bottom distributions together with the fully convoluted F_2^c and F_2^b structure functions which are also compared with the NLO ones. In general the NNLO results for $F_2^{c,b}$ fall below the NLO ones (dash-dotted curves) in the small-x region. Here at NNLO the $\mathcal{O}(\alpha_s^2)$ convolutions of the fermionic and gluonic coefficient functions with $\overset{(-)}{h}$ and the gluon distribution, respectively, become more important than at NLO since the "heavy" quark distributions xc and xb by themselves (short-dashed curves) are sizably different from $\frac{9}{8}F_2^c$ and $\frac{9}{2}F_2^b$, respectively. At NLO the $\mathcal{O}(\alpha_s)$ quark and gluon convolution contributions almost cancel [12] and thus xc and xb almost coincide with the appropriate NLO structure functions in Fig. 1. As is obvious from Fig. 1, however, such differences between NNLO and NLO results lie always within the 1σ–2σ uncertainty bands in the relevant large Q^2 region, $Q^2 \gtrsim 10^2$–10^3 GeV^2, and can therefore be hardly delineated experimentally.

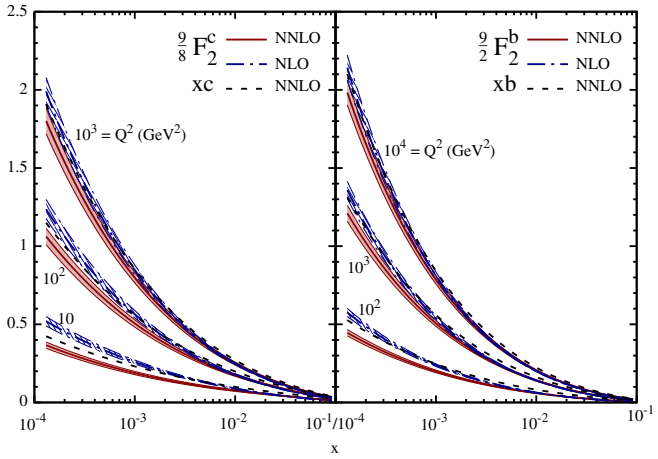

FIG. 1 (color online). The predicted x dependencies of the charm and bottom-quark structure functions $\frac{9}{8}F_2^c(x, Q^2)$ and $\frac{9}{2}F_2^b(x, Q^2)$, respectively, in the zero-mass VFNS, together with their $\pm 1\sigma$ uncertainties, at some typical fixed values of Q^2. The NNLO charm and bottom distributions, $xc(x, Q^2)$ and $xb(x, Q^2)$, are shown by the short-dashed curves.

The shape of the gluon distribution at two typical fixed values of x, relevant for Higgs-boson production at LHC, is illustrated in Fig. 2. At small to medium values of Q^2 the NNLO gluon falls always *below* the NLO one and in both orders the gluon remains positive at small Q^2 in the very small-x region. This dampening of the NNLO gluon is a typical NNLO effect being mainly caused [1] by the gluonic 3-loop splitting function $P_{gg}^{(2)}$ which is *negative* and *more* singular ($\sim -\frac{1}{x}\ln\frac{1}{x}$) in the small-$x$ region [31] than in the NLO (and LO) ones. At large values of Q^2 the NNLO and NLO gluon distributions become practically indistinguishable.

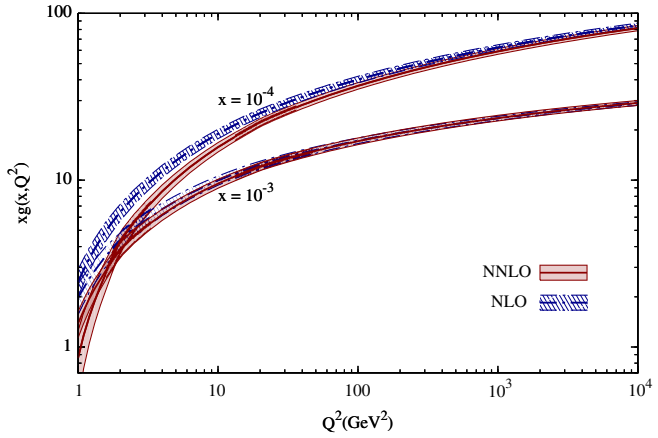

FIG. 2 (color online). The NNLO and NLO gluon distributions together with their $\pm 1\sigma$ uncertainty bands at two representative fixed values of x.

A. Weak gauge boson production

As a next test of our VFNS distributions we turn to the hadronic $W^{\pm}$ and Z^0 production. The inclusive differential cross section is usually written as [32]

$$\frac{d\sigma^V}{dQ^2} = \tau\sigma_V(Q^2, M_V^2)W_V(\tau, Q^2), \qquad \tau = Q^2/s, \quad (5)$$

where V is one of the gauge bosons of the standard model (γ, Z^0, or $W^{\pm}$) which subsequently decays into a lepton pair ($\ell_1\ell_2$) with invariant mass $M_{\ell_1\ell_2}$, i.e. $Q^2 \equiv M^2_{\ell_1\ell_2}$, and σ_V is the pointlike cross section, e.g., $\sigma_\gamma = 4\pi\alpha^2/9Q^4$, etc. [32]. The hadronic Drell-Yan structure function is represented by

$$W_V(\tau, Q^2) = \sum_{i,j}\int_\tau^1 \frac{dx_1}{x_1}\int_{\tau/x_1}^1 \frac{dx_2}{x_2} PD_{ij}^V(x_1, x_2, \mu_F^2) \times \Delta_{ij}\left(\frac{\tau}{x_1x_2}, Q^2, \mu_F^2\right), \quad (6)$$

with PD_{ij}^V denoting the usual combination of pdfs of flavor types i and j which depend on the factorization scale μ_F. The QCD correction term is expanded in a power series of α_s (or $\alpha_s/4\pi$ or α_s/π) as follows:

$$\Delta_{ij}(x, Q^2, \mu_F^2) = \sum_{n=0}^{2}\alpha_s^n(\mu_R^2)\Delta_{ij}^{(n)}(x, Q^2, \mu_F^2, \mu_R^2), \quad (7)$$

with $\Delta_{ij}^{(1)}$ and the NNLO 2-loop $\Delta_{ij}^{(2)}$ being given in [32,33], and the choice for the renormalization scale $\mu_R = \mu_F$ is dictated by all presently available pdfs which have been determined and evolved according to $\mu_R = \mu_F$. The scale uncertainties of our predictions are defined by taking $M_W/2 \le \mu_F \le 2M_W$, using $M_W = 80.4$ GeV (and similarly for Z^0 production, using $M_Z = 91.2$ GeV). Furthermore, it should be noted that only the initial u, d, s, c quark flavors and the gluon contribute sizably via the various fusion subprocesses in (6) to the production rates of gauge bosons, whereas all subprocesses involving the b-flavor distribution, e.g., $u\bar{b} \to W^+$, $\bar{c}b \to W^-$, etc., are negligibly small [12].

Our NNLO predictions for $\sigma(p\bar{p} \to W^{\pm}X)$ and $\sigma(p\bar{p} \to Z^0X)$ are compared with our NLO ones [12] in Fig. 3 where, for comparison, we also show the predictions of Alekhin [14,34]. The vector boson production rates at NNLO are typically slightly *larger* (by more than 1σ than at NLO with a $K \equiv$ NNLO/NLO factor of $K^{W^+ + W^-} = 1.04$ and $K^{Z^0} = 1.06$ at Tevatron energies ($\sqrt{s} = 1.96$ TeV, cf. Table I) to be compared with the predictions of Alekhin [14,34] $K_A^{W^+ + W^-} \simeq K_A^{Z^0} = 1.03$. This confirms again the fast perturbative convergence at NNLO since the NLO/LO K factor[12] is 1.3 for $W^+ + W^-$ production at $\sqrt{s} = 1.96$ TeV. Our predicted NNLO cross sections at $\sqrt{s} = 1.96$ TeV (cf. Table I), $\sigma(p\bar{p} \to W^+ + W^- + X) = 25.2$ nb, and $\sigma(p\bar{p} \to Z^0 + X) = 7.5$ nb, are similar to the ones of Martin, Stirling, Thorne, and Watt [39], 25.4 nb and 7.4 nb, respectively, but smaller than the ones obtained by Alekhin [34], 25.8 nb and 7.8 nb, respectively. For the latter cases the branching ratios $B(W \to \ell\nu) = 0.108$ and $B(Z \to \ell^+\ell^-) = 0.034$ have been used. It is obvious from Fig. 3 that most of these results are within the present experimental 1σ uncertainty. The scale uncertainties of our NNLO predictions in Fig. 3 at $\sqrt{s} = 1.96$ TeV amount to less than 0.5% (where $\mu_F = M_V/2$ gives rise to the upper limits and $\mu_F = 2M_V$ to the lower limits, with $V = W^{\pm}, Z^0$) which is 4 times less than at NLO [12].

In Table II we present our NNLO predictions for $W^{\pm}$ and Z^0 production at LHC energies. For comparison we also display our previous NLO results [12]. Here the scale uncertainties amount to less than 1.7%, i.e., are about half

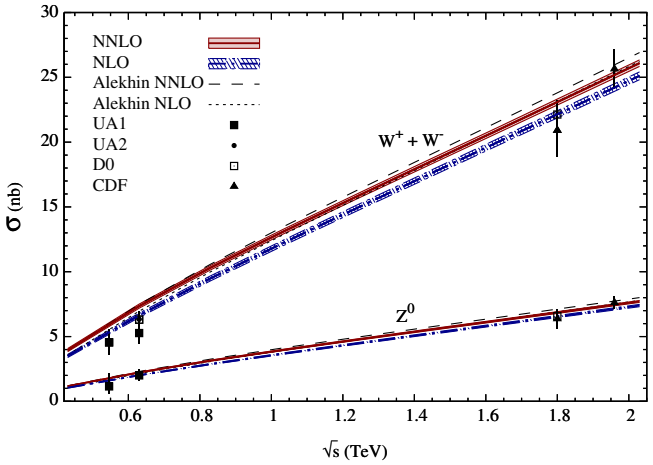

FIG. 3 (color online). Predictions for the total $W^+ + W^-$ and Z^0 production rates at $p\bar{p}$ colliders with the data taken from [35–38]. Our NLO VFNS predictions are taken from [12], and the NLO and NNLO ones of Alekhin from [14,34]. The adopted momentum scale is $\mu_F = \mu_R = M_V$ for $V = W^{\pm}, Z^0$. The scale uncertainties of our NNLO predictions, due to $\frac{1}{2}M_V \le \mu_F \le 2M_V$, amount to less than 0.5% at $\sqrt{s} = 1.96$ TeV, i.e., is 4 times less than at NLO [12]. The shaded band around our NNLO and NLO predictions are due to the $\pm 1\sigma$ uncertainty implied by our dynamical NNLO [1] and NLO [7] parton distributions.

TABLE I. NNLO predictions for vector boson production at the Tevatron, with the NLO ones being taken from [12]. The errors refer to the $\pm 1\sigma$ uncertainties implied by our dynamical NNLO [1] and NLO [7] pdfs. The scale uncertainties of our NNLO predictions, due to $\frac{1}{2}M_V \le \mu_F \le 2M_V$, amount to less than 0.5% (i.e., are about half as large as the stated pdf uncertainties) which is about 4 times smaller than at NLO [12].

$\sigma^{p\bar{p}\to VX}$ (nb), $\sqrt{s} = 1.96$ TeV		
V	NNLO	NLO
$W^{\pm}$	12.6 ± 0.1	12.1 ± 0.1
$W^+ + W^-$	25.2 ± 0.3	24.2 ± 0.3
Z^0	7.5 ± 0.1	7.1 ± 0.1

TABLE II. As in Table I but for LHC energies. The scale uncertainties of our NNLO predictions amount to less than 1.7% of the total predicted rates which is about half as large as the stated pdf 1σ uncertainties and the scale uncertainties at NLO [12].

$\sigma^{pp\to VX}$ (nb), $\sqrt{s} = 10$ TeV		
V	NNLO	NLO
W^+	78.7 ± 2.0	76.7 ± 1.7
W^-	55.8 ± 1.4	54.7 ± 1.2
$W^+ + W^-$	134.5 ± 3.4	131.6 ± 2.9
Z^0	39.1 ± 0.9	38.1 ± 0.8
$\sigma^{pp\to VX}$ (nb), $\sqrt{s} = 14$ TeV		
V	NNLO	NLO
W^+	109.8 ± 3.2	107.5 ± 2.9
W^-	80.4 ± 2.4	79.1 ± 2.1
$W^+ + W^-$	190.2 ± 5.6	186.5 ± 4.9
Z^0	55.7 ± 1.5	54.6 ± 1.3

as large than the stated pdf uncertainties and than the scale uncertainties at NLO [12]. For example, the full NNLO expectations at $\sqrt{s} = 14$ TeV are

$$\sigma(pp \to W^+ + W^- + X) = 190.2 \pm 5.6_{\text{pdf}} \, {}^{+1.6}_{-1.2}|_{\text{scale}} \text{ nb}, \tag{8}$$

$$\sigma(pp \to Z^0 + X) = 55.7 \pm 1.5_{\text{pdf}} \, {}^{+0.6}_{-0.3}|_{\text{scale}} \text{ nb}. \tag{9}$$

Here the scale choice $\mu_F = 2M_V$ gives rise to the upper limits, and $\mu_F = M_V/2$ to the lower limits of our predicted cross sections. These results are about 5% smaller than the ones of Martin, Stirling, Thorne, and Watt [39], whereas Alekhin [34] obtained 195.2 nb and 57.7 nb for $W^+ + W^-$ and Z^0 production, respectively, with similar pdf uncertainties as in (8) and (9). From Table II it becomes obvious that the vector boson production rates somewhat increase at NNLO as compared to the NLO expectations, but such differences are well within present pdf and scale uncertainties. Moreover, the smallness of such differences ($K \simeq 1.02$) indicates the reliability of perturbative predictions already at NLO. For comparison we note that within the FFNS (where the heavy c, b, t quark flavors do not form massless partons of the nucleon) the $W^+ + W^-$ production rate has been estimated [12] to be about 192.7 nb at NLO with a total (pdf as well as scale) uncertainty of about 5% at $\sqrt{s} = 14$ TeV. In general the NLO-VFNS prediction of 186.5 nb in Table II falls somewhat below that estimate but remains well within its total uncertainty of about 6% [12]. Because of the reduced scale ambiguity at NNLO and due to the slightly different NNLO estimates obtained by other groups as discussed above, we conclude that the rates for gauge boson production at LHC energies can be rather confidently predicted with an accuracy of about 5% irrespective of the factorization scheme.

B. Higgs-boson production

As a final application of our NNLO-VFNS pdfs we consider the hadronic production of the SM Higgs boson. Similar as for gauge boson production in Sec. II A, the total inclusive cross section for Higgs-boson production is usually written as [32,33,40,41]

$$\sigma^H(s) = \sum_{i,j} \int_0^1 dx_1 dx_2 PD_{ij}^H(x_1, x_2, \mu_F^2) \times \hat{\sigma}_{ij\to H}(\hat{s} = x_1 x_2 s, \mu_F^2, \mu_R^2), \tag{10}$$

with the partonic cross sections for $ij \to HX$ being written as

$$\hat{\sigma}_{ij\to H}(\hat{s}) = \sigma_0 \Delta_{ij}(\hat{s}) = \sigma_0 \sum_{n=0}^{2} \alpha_s^n(\mu_R^2) \Delta_{ij}^{(n)}(\hat{s}, \mu_F^2, \mu_R^2), \tag{11}$$

where the obvious μ_F and μ_R dependencies have been suppressed. The dominant Higgs production proceeds via gluon-gluon fusion where $\sigma_0 = \alpha_s^2/(576\pi v^2)$ for the initial LO process $gg \to H$, with the Higgs vacuum expectation value $v = (\sqrt{2}G_F)^{-1/2} \simeq 246$ GeV, and the NLO QCD corrections $\Delta_{ij}^{(1)}$ are given in [42,43] and the NNLO $\Delta_{ij}^{(2)}$ ones in [33,40]. The factorization scale is usually chosen to be $\mu_F = M_H$, and the scale uncertainty is illustrated by taking $\frac{1}{2}M_H \le \mu_F \le 2M_H$. The much smaller contribution stemming from bottom-quark annihilation starts at LO with $b\bar{b} \to H$ where $\sigma_0 = \pi\lambda_b^2/(12M_H^2)$ with $\lambda_b = \sqrt{2}m_b/v$ in the SM, and the NLO and NNLO-QCD corrections $\Delta_{ij}^{(1)}$ and $\Delta_{ij}^{(2)}$ can be found in [41]. Here it has been argued [44–46] that the optimal choice of the factorization scale is $\mu_F \simeq M_H/4$ where the differences between the VFNS and the FFNS are significantly reduced and the LO, NLO, and NNLO results become rather similar [41], which implies a more stable perturbative behavior. The scale uncertainty is again probed by taking $\frac{1}{2} \times (M_H/4) \le \mu_F \le 2(M_H/4)$. In both cases $\mu_R = \mu_F$ as dictated by all presently available pdfs.

In Fig. 4 we show, as a function of the Higgs mass, our NNLO (thick solid curve) and NLO (thick dash-dotted curve) predictions for LHC for Higgs-boson production via the dominant gluon-gluon fusion subprocess which starts, at LO, with $gg \to H$. The shaded regions around these central predictions are due to the $\pm 1\sigma$ pdf uncertainties. Reducing the scale to $\frac{1}{2}M_H$ one arrives at the thin upper curves at each order, whereas the scale choice $\mu_F = 2M_H$ results in the respective lower curves, where the appropriate $\pm 1\sigma$ pdf ambiguities have also been included for each choice of scale. These ambiguities for each scale choice $\mu_F = \mu_R = \frac{1}{2}M_H$, M_H, $2M_H$ are more explicitly

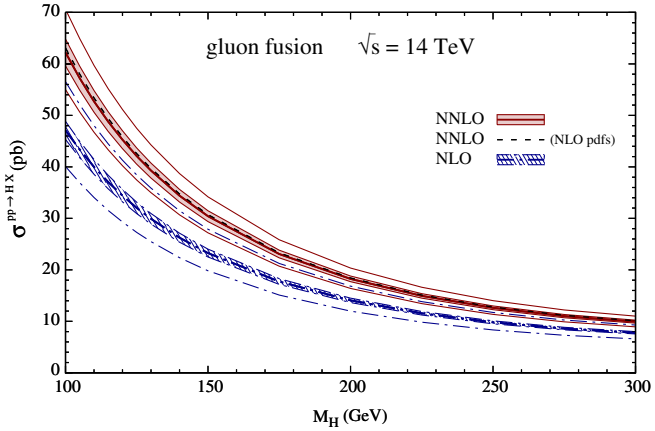

FIG. 4 (color online). Predictions for SM Higgs-boson production at LHC ($pp \to HX$) via the dominant gluon-gluon fusion process, which starts at LO with $gg \to H$ via a top-quark loop. The shaded bands around the central NNLO and NLO predictions are due to the $\pm 1\sigma$ pdf uncertainties, all referring to a scale choice $\mu_F = \mu_R = M_H$. The thin solid and dash-dotted curves above these NNLO and NLO bands refer to a scale $\mu_F = \mu_R = \frac{1}{2}M_H$ with $\pm 1\sigma$ pdf uncertainties included, and similarly the lower curves refer to $\mu_F = \mu_R = 2M_H$ (for more details cf. Table III). The dashed NNLO curve is obtained by using NNLO matrix elements and (inconsistently) NLO pdfs [12] with $\mu_F = \mu_R = M_H$.

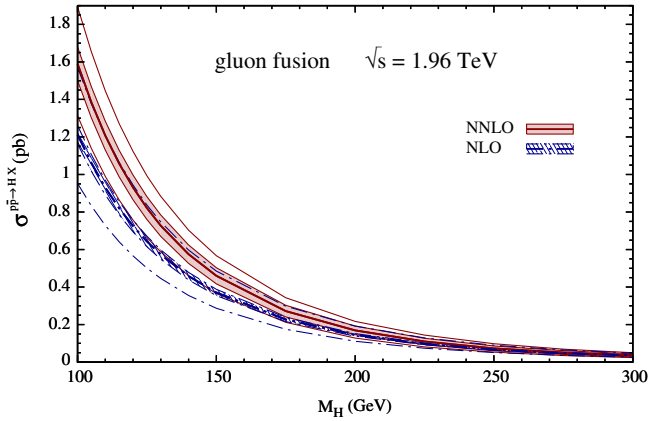

FIG. 5 (color online). As in Fig. 4 but for the Tevatron ($p\bar{p} \to HX$).

illustrated in Table III. Despite the fact that the NLO and NNLO total uncertainty bands overlap in Fig. 4, the predicted NNLO production rates are typically about 20% larger than at NLO. The insensitivity of these predictions with respect to the appropriate choice of the pdfs is illustrated by the dashed curve which has been obtained by using NNLO matrix elements and (inconsistently) NLO pdfs. Here for the dominant gluon fusion process such an inconsistent choice of the pdfs appears to be immaterial and the production rates depend dominantly on the NNLO QCD dynamics. Our central predictions in Fig. 4 are comparable with the ones presented in [47], but are about 10% smaller than the ones in [39]. For completeness we also show in Fig. 5 our NNLO expectations for Higgs-boson production at the Tevatron, $\sqrt{s} = 1.96$ TeV. Note that here the total uncertainty bands almost double at NNLO and NLO as compared to the ones at LHC in Fig. 4.

In Fig. 6 we finally show the subdominant contribution to Higgs-boson production at LHC due to bottom-quark fusion which starts with $b\bar{b} \to H$ at LO. Here, in contrast to the by far dominant gluon fusion process in Fig.4, the NNLO and NLO predictions, together with their $\pm 1\sigma$ pdf uncertainties, almost coincide with the NNLO results falling very slightly below the NLO ones. Here, however, the correct choice of the NNLO pdfs turns out to be important, since choosing (incorrectly) NLO pdfs [12] for a NNLO analysis results in too small a production rate as shown by the dashed curve. At NNLO the scale dependence is here, again in contrast to the by far dominant gluon-gluon fusion

TABLE III. Typical NNLO scale dependencies of the cross sections (in units of pb) for Higgs-boson producion at $\sqrt{s} = 14$ TeV via the dominant gluon-gluon fusion subprocess with M_H in GeV units. The errors refer to the 1σ pdf uncertainties. The maximal upper limits at $\mu_F = \mu_R = \frac{1}{2}M_H$ agree with the thin solid curve at NNLO in Fig. 4, whereas the lower curve in Fig. 4 corresponds to the minimal lower limits at $\mu_F = \mu_R = 2M_H$.

$M_H \backslash \mu_F$	$\frac{1}{2}M_H$	M_H	$2M_H$
100	67.6 ± 3.0	62.2 ± 2.6	57.3 ± 2.2
150	33.0 ± 1.2	30.4 ± 1.0	28.1 ± 0.9
200	19.7 ± 0.6	18.3 ± 0.5	16.9 ± 0.5
250	13.6 ± 0.4	12.6 ± 0.4	11.7 ± 0.3
300	10.7 ± 0.3	9.9 ± 0.3	9.2 ± 0.3

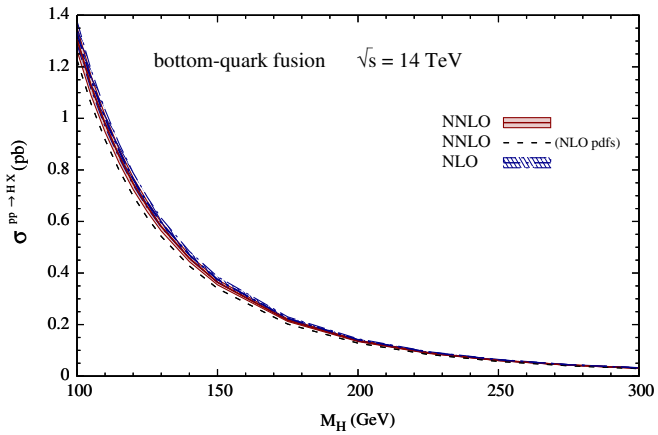

FIG. 6 (color online). Predictions for SM Higgs-boson production at LHC via the small subdominant bottom-quark fusion process which starts with $b\bar{b} \to H$ at LO. The shaded bands correspond to the $\pm 1\sigma$ pdf uncertainties of the NNLO and NLO central predictions, all referring to a scale choice $\mu_F = \mu_R = M_H/4$. The dashed NNLO curve is obtained by using NNLO matrix elements and (inconsistently) NLO pdfs [12].

process, very marginal: using $\mu_F = \mu_R = 2(M_H/4)$ instead of $M_H/4$ leaves the results in Fig. 6 practically unchanged, whereas the choice $\mu_F = \mu_R = \frac{1}{2}(M_H/4)$ increases the results by at most 5%.

It should be again emphasized that here, as in the previous case of gauge boson production, the simpler VFNS yields sufficiently reliable predictions for Higgs-boson production despite the fact that a fully massive FFNS analysis cannot be performed at NNLO at present (due to the absence of NNLO, and in many cases even NLO, matrix elements with $m_h \neq 0$). This is due to the fact that $\sqrt{\hat{s}_{\rm th}}/m_b = (2m_b + M_H)/m_b \gg 1$, i.e., nonrelativistic contributions from the threshold region in the FFNS are suppressed, and thus the FFNS and VFNS predictions should not differ too much [12], as has been discussed in more detail in the Introduction. Indeed it has been noted [12] that the FFNS and VFNS results at NLO are compatible [48–50], and that the VFNS rates exceed the corresponding FFNS Higgs-boson production rates by about 10–20%, depending on the choice of the scale $\mu_F = \mu_R$.

III. SUMMARY AND CONCLUSIONS

Based on our recent NNLO dynamical parton distributions as obtained in the FFNS [1], we generated radiatively VFNS parton distributions at NNLO where the heavy-quark flavors (c, b, t) also become massless partons within the nucleon. The latter pdfs in the ''variable flavor number'' factorization scheme considerably ease the otherwise unduly complicated calculations in the FFNS where for the time being fully massive NNLO analyses are not possible (and in many cases even not at NLO), such as the calculation of gauge- and Higgs-boson production and heavy-quark production at collider energies. It has been shown [12] that for situations where the invariant mass of the produced system exceeds by far the mass of the participating heavy flavor in the FFNS, the VFNS predictions deviate rather little from the FFNS ones, typically by about 10% which is within the margins of renormalization and factorization scale uncertainties and ambiguities related to presently available parton distributions. As an application of our NNLO-VFNS pdfs we studied the perturbative stability of the predictions for gauge ($W^{\pm}$, Z^0) and SM Higgs-boson production at collider energies by comparing them with the appropriate NLO results, taking into account pdf uncertainties as well as scale dependencies. The NNLO predictions for gauge boson production are typically slightly larger (by more than 1σ) than the NLO ones, cf. Tables I and II. Because of the reduced scale ambiguity at NNLO and due to the slightly different NNLO estimates of other groups we conclude that the rates for gauge boson production at LHC energies can be rather confidently predicted with an accuracy of about 5%. At the Tevatron ($\sqrt{s} = 1.96$ TeV) the NNLO predictions are more than a 2σ pdf uncertainty above the NLO ones, but most of these results are within the present experimental 1σ uncertainty.

The NNLO predictions for the production of the SM Higgs boson via the dominant gluon fusion (in contrast to the subdominant bottom-quark fusion) process are, at collider energies, typically about 20% larger than at NLO, but their respective total (pdf and scale) uncertainty bands overlap. Higgs-boson production at LHC ($\sqrt{s} = 14$ TeV) can be predicted with an accuracy of about 10% at NNLO (with the total uncertainty being almost twice as large at NLO), whereas the uncertainty almost doubles at Tevatron ($\sqrt{s} = 1.96$ TeV).

A FORTRAN code (grid) containing our NNLO-VFNS pdfs (including their uncertainties) can be obtained on request or directly online from [52].

ACKNOWLEDGMENTS

We are grateful to R. Harlander for providing us with the NNLO routine for calculating hadronic Higgs-boson production cross sections, as well as for a clarifying correspondence. We also thank J. Blümlein and M. Glück for helpful discussions and comments. This work has been supported in part by the ''Bundesministerium für Bildung und Forschung,'' Berlin/Bonn.

Note added in proof.—While completing this manuscript, an investigation along similar lines appeared [53]. Several results are similar to ours. However, the gauge boson production rates are about 4% larger at the Tevatron and about 10% larger at LHC than our NNLO predictions. Similarly, the NNLO predictions for Higgs-boson production at LHC ($\sqrt{s} = 14$ TeV) are 5–8% larger for $M_H \lesssim 150$ GeV than ours, but agree with us for larger Higgs masses, whereas at the Tevatron their expected rates are 12–30% smaller than ours for $M_H = 100$–200 GeV. The comparison of these production rates refers always to the central results, disregarding all pdf and scale uncertainties.

APPENDIX

Some analytic form of the Mellin n moments of the operator matrix elements including the heavy-quark flavors, which have been originally calculated in Bjorken-x space [16] and which are needed in (1)–(3) have been already implicitly used in some NNLO evolution programs (see, e.g. [51]). Here we summarize the relevant analytic expressions which can be directly continued to complex values of n as required for the Mellin inversions to Bjorken-x space.

The Bjorken-x expressions are given in Appendix B of [16] and we follow the notation used there [cf. also (1)–(3)]. Because of our choice $Q^2 = m_h^2$ for the flavor transition thresholds, only the scale-independent parts of these expressions contribute. Their moments are as follows:

$$\frac{1}{C_F T_f}\tilde{A}_{hq}^{PS,(2)}(n) = -8\frac{n^4+2n^3+5n^2+4n+4}{(n-1)n^2(n+1)^2(n+2)}S_2(n-1) - \frac{448}{27}\frac{1}{n-1} - \frac{44}{n} + \frac{48}{n^2} - \frac{4}{n^3} + \frac{24}{n^4} - \frac{12}{n+1} + \frac{56}{(n+1)^2} + \frac{28}{(n+1)^3} + \frac{24}{(n+1)^4} + \frac{1960}{27}\frac{1}{n+2} + \frac{448}{9}\frac{1}{(n+2)^2} + \frac{64}{3}\frac{1}{(n+2)^3}, \tag{A1}$$

where $C_F = \frac{4}{3}$, $T_f = \frac{1}{2}$ and $S_k(n) \equiv \sum_{j=1}^{n}\frac{1}{j^k}$ using

$$S_1(n) = \psi(n+1) + \gamma_E, \qquad S_{k'}(n) = \frac{(-1)^{k'-1}}{(k'-1)!}\psi^{(k'-1)}(n+1) + \zeta(k'), \quad k' \geq 2, \tag{A2}$$

with $\psi^{(i)}(z) = d^{(i+1)}\ln\Gamma(z)/dz^{i+1}$ and $\gamma_E = 0.577\,215\,664\,9$, $\zeta(2) = \pi^2/6$ and $\zeta(3) = 1.202\,056\,903\,2$ for the analytic continuation to complex n. Since the moment of the rather complicated coefficient $\tilde{A}_{hg}^{S,(2)}$ appearing in (1), and as given in (B.3) of [16], cannot be straightforwardly expressed in terms of analytic functions of n [8], we have employed for practical purposes the n moment of the sufficiently accurate x parametrization suggested in [51]

$$\tilde{A}_{hg}^{S,(2)}(n) = 1.111\frac{S_1^3(n)}{n} - 0.4\frac{S_1^2(n)}{n} + \left(\frac{2.77}{n} + \frac{293.6}{n^3}\right)S_1(n) + \frac{3.333}{n}S_1(n)S_2(n) - \left(\frac{0.4}{n} - \frac{293.6}{n^2}\right)S_2(n) + 295.822\frac{S_3(n)}{n} - 0.006 - \frac{24.89}{n-1} - \frac{187.8+293.6\zeta(3)}{n} + \frac{93.68-293.6\zeta(2)}{n^2} - \frac{6.584}{n^3} + \frac{9.336}{n^4} + \frac{249.6}{n+1}. \tag{A3}$$

The remaining coefficients relevant for the light quark and gluon sector in (2) and (3) respectively, can be straightforwardly transformed to n space:

$$\frac{1}{C_F T_f}A_{qq,h}^{\mathrm{NS},(2)}(n) = -\frac{224}{27}S_1(n-1) + \frac{40}{9}S_2(n-1) - \frac{8}{3}S_3(n-1) + \frac{73}{18} + \frac{44}{27}\frac{1}{n} - \frac{4}{9}\frac{1}{n^2} - \frac{268}{27}\frac{1}{n+1} + \frac{44}{9}\frac{1}{(n+1)^2} - \frac{4}{3}\frac{1}{n^3} - \frac{4}{3}\frac{1}{(n+1)^3}. \tag{A4}$$

$$\frac{1}{C_F T_f}A_{gq,h}^{S,(2)}(n) = \frac{8}{3}\frac{1}{n-1}\left[S_1^2(n-1) - \frac{10}{3}S_1(n-1) + S_2(n-1) + \frac{56}{9}\right] - \frac{8}{3}\frac{1}{n}\left[S_1^2(n) - \frac{10}{3}S_1(n) + S_2(n) + \frac{56}{9}\right] + \frac{4}{3}\frac{1}{n+1}\left[S_1^2(n+1) - \frac{16}{3}S_1(n+1) + S_2(n+1) + \frac{86}{9}\right], \tag{A5}$$

$$A_{gg,h}^{S,(2)}(n) = 4C_F T_f\left[-\frac{15}{4} - \frac{2}{n-1} + \frac{20}{n} - \frac{8}{n^2} + \frac{3}{n^3} - \frac{2}{n^4} - \frac{12}{n+1} - \frac{12}{(n+1)^2} + \frac{5}{(n+1)^3} - \frac{2}{(n+1)^4} - \frac{6}{n+2}\right] + 4C_A T_f\left[-\frac{56}{27}S_1(n-1) + \frac{1}{3}\frac{S_1(n+1)}{n+1} + \frac{5}{18} + \frac{139}{27}\frac{1}{n-1} - \frac{157}{27n} - \frac{13}{9n^2} + \frac{2}{3n^3} + \frac{137}{27}\frac{1}{n+1} - \frac{22}{9}\frac{1}{(n+1)^2} + \frac{2}{3}\frac{1}{(n+1)^3} - \frac{175}{27}\frac{1}{n+2}\right]. \tag{A6}$$

with $C_A = 3$.

[1] P. Jimenez-Delgado and E. Reya, Phys. Rev. D **79**, 074023 (2009).
[2] S. Chekanov *et al.* (ZEUS Collaboration), Phys. Rev. D **69**, 012004 (2004).
[3] C. Adloff *et al.* (H1 Collaboration), Phys. Lett. B **528**, 199 (2002).
[4] A. Aktas *et al.* (H1 Collaboration), Eur. Phys. J. C **40**, 349 (2005).
[5] A. Aktas *et al.* (H1 Collaboration), Eur. Phys. J. C **45**, 23 (2006).
[6] M. Glück, E. Reya, and A. Vogt, Eur. Phys. J. C **5**, 461 (1998).
[7] M. Glück, P. Jimenez-Delgado, and E. Reya, Eur. Phys. J. C **53**, 355 (2008).
[8] J. Blümlein, A. De Freitas, W. L. van Neerven, and S. Klein, Nucl. Phys. **B755**, 272 (2006).

[9] I. Bierenbaum, J. Blümlein, and S. Klein, Acta Phys. Pol. B **38**, 3543 (2007).
[10] I. Bierenbaum, J. Blümlein, S. Klein, and C. Schneider, Nucl. Phys. **B803**, 1 (2008).
[11] I. Bierenbaum, J. Blümlein, and S. Klein, Nucl. Phys. **B820**, 417 (2009).
[12] M. Glück, P. Jimenez-Delgado, E. Reya, and C. Schuck, Phys. Lett. B **664**, 133 (2008).
[13] J. Pumplin *et al.* (CTEQ6 Collaboration), J. High Energy Phys. 07 (2002) 012.
[14] S. I. Alekhin, Phys. Rev. D **68**, 014002 (2003).
[15] M. A. G. Aivaizis, J. C. Collins, F. Olness, and W. K. Tung, Phys. Rev. D **50**, 3102 (1994).
[16] M. Buza, Y. Matiounine, J. Smith, and W. L. van Neerven, Eur. Phys. J. C **1**, 301 (1998).
[17] R. S. Thorne and R. G. Roberts, Phys. Rev. D **57**, 6871 (1998).
[18] A. Chuvakin, J. Smith, and W. L. van Neerven, Phys. Rev. D **61**, 096004 (2000).
[19] M. Krämer, F. I. Olness, and D. E. Soper, Phys. Rev. D **62**, 096007 (2000).
[20] A. D. Martin, R. G. Roberts, W. J. Stirling, and R. S. Thorne, Eur. Phys. J. C **23**, 73 (2002).
[21] A. D. Martin, R. G. Roberts, W. J. Stirling, and R. S. Thorne, Phys. Lett. B **531**, 216 (2002).
[22] W. K. Tung, S. Kretzer, and C. Schmidt, J. Phys. G **28**, 983 (2002).
[23] S. Kretzer *et al.*, Phys. Rev. D **69**, 114005 (2004).
[24] R. S. Thorne, Phys. Rev. D **73**, 054019 (2006).
[25] W. K. Tung *et al.* (CTEQ6.5 Collaboration), J. High Energy Phys. 02 (2007) 053.
[26] A. Vogt, arXiv:0707.4106.
[27] R. S. Thorne and W. K. Tung, arXiv:0809.0714.
[28] P. M. Nadolsky and W. K. Tung, Phys. Rev. D **79**, 113014 (2009).
[29] T. Stelzer, Z. Sullivan, and S. Willenbrock, Phys. Rev. D **56**, 5919 (1997).
[30] I. Bierenbaum, J. Blümlein, and S. Klein, Phys. Lett. B **672**, 401 (2009).
[31] A. Vogt, S. Moch, and J. A. M. Vermaseren, Nucl. Phys. **B691**, 129 (2004).
[32] R. Hamberg, W. L. van Neerven, and T. Matsuura, Nucl. Phys. **B359**, 343 (1991); **B644**, 403(E) (2002).
[33] R. V. Harlander and W. B. Kilgore, Phys. Rev. Lett. **88**, 201801 (2002).
[34] S. I. Alekhin, JETP Lett. **82**, 628 (2005).
[35] C. Albajar *et al.* (UA1 Collaboration), Z. Phys. C **44**, 15 (1989).
[36] J. Alitti *et al.* (UA2 Collaboration), Phys. Lett. B **276**, 365 (1992).
[37] B. Abbott *et al.* (D0 Collaboration), Phys. Rev. D **61**, 072001 (2000).
[38] F. Abe *et al.* (CDF Collaboration), Phys. Rev. Lett. **69**, 28 (1992); A. Abulencia *et al.* (CDF Collaboration), J. Phys. G **34**, 2457 (2007).
[39] A. D. Martin, W. J. Stirling, R. S. Thorne, and G. Watt, arXiv:0905.3531.
[40] C. Anastasiou and K. Melnikov, Nucl. Phys. **B646**, 220 (2002); V. Ravindran, J. Smith, and W. L. van Neerven, *ibid.***B665**, 325 (2003).
[41] R. V. Harlander and W. B. Kilgore, Phys. Rev. D **68**, 013001 (2003).
[42] S. Dawson, Nucl. Phys. **B359**, 283 (1991).
[43] A. Djouadi, M. Spira, and P. M. Zerwas, Phys. Lett. B **264**, 440 (1991).
[44] T. Plehn, Phys. Rev. D **67**, 014018 (2003).
[45] F. Maltoni, Z. Sullivan, and S. Willenbrock, Phys. Rev. D **67**, 093005 (2003).
[46] E. Boos and T. Plehn, Phys. Rev. D **69**, 094005 (2004).
[47] R. Harlander, J. Phys. G **35**, 033001 (2008).
[48] S. Dittmaier, M. Krämer, and M. Spira, Phys. Rev. D **70**, 074010 (2004).
[49] J. Campbell *et al.*, arXiv:hep-ph/0405302.
[50] S. Dawson, C. B. Jackson, L. Reina, and D. Wackeroth, Mod. Phys. Lett. A **21**, 89 (2006).
[51] A. Vogt, Comput. Phys. Commun. **170**, 65 (2005).
[52] P. Jimenez-Delgado and E. Reya, http://doom.physik.uni-dortmund.de/pdfserver.
[53] S. Alekhin, J. Blümlein, S. Klein, and S. Moch, arXiv:0908.2766.